Hindawi
International Journal of Photoenergy
Volume 2020, Article ID 8840411, 8 pages
https://doi.org/10.1155/2020/8840411

Research Article

Effect of Chemical and Physical Parameters on the Electrical Outputs of $Cu_2Zn_{1-y}Fe_ySnS_4$-Based Solar Cells by wxAMPS

Hervé Joël Tchognia Nkuissi,[1,2,3] **Luc Leroy Mambou Ngueyep**,[1,2] **Abdouramani Dadjé**,[1] **Guy Molay Tchapga Gnamsi**,[1,2] **André Chamgoué Chéagé**,[1] **Bouchaib Hartiti**,[3] **and Jean-Marie Ndjaka**[2]

[1]*School of Geology and Mining Engineering, University of Ngaoundéré, P.O. Box 115, Meiganga, Cameroon*
[2]*Department of Physics, Faculty of Science, University of Yaoundé I, P.O. Box 812, Yaoundé, Cameroon*
[3]*ERDyS Laboratory, Materials, Energy, Water, Modeling and Sustainable Development Group, Faculty of Science and Technique, Hassan II University of Casablanca, Mohammedia, Morocco*

Correspondence should be addressed to Hervé Joël Tchognia Nkuissi; hervetchognia@gmail.com

Received 17 July 2020; Accepted 13 September 2020; Published 22 September 2020

Academic Editor: Adel A. Ismail

$Cu_2Zn_{1-y}Fe_ySnS_4$-based solar cells with different mole fractions of iron have been analyzed using numerical simulations in this study. The analysis deals with the effect of the iron content on the overall electrical performance of solar cells. Results revealed that the Voc is affected by the increase of the iron content even if it improves the other parameters. We found that the CZFTS solar cell with a mole fraction of iron equal to 1 (CFTS) showed the best results in terms of power conversion efficiency (PCE). Moreover, variations of several structural and physical parameters of the buffer CdS and the best absorber CFTS on the overall electrical characteristics of the cell were investigated. Simulations showed promising results with PCE of 20.35%, Jsc of 26.09 mA/cm^2, Voc of 0.93 V, and FF of 83.93%. The results obtained can serve as a basis for the design and manufacture of high-efficiency CZFTS solar cells.

1. Introduction

Recently, earth-abundant $Cu_2ZnSn(S, Se)_4$ nanocrystals are being considered as alternative and ideal absorber materials to CIGS and for thin-film solar cells, thanks to their large absorption coefficients and their tunable direct bandgap energy ranging from 1.0 to 1.5 eV [1–10]. On the other hand, earth-abundant Cu_2II-IV-$(S, Se)_4$ (II = Mn, Fe, Co, Ni, Hg; IV = Si, Ge, Sn) chalcogenide semiconductor nanocrystals have gained broad interest due to their analogous structures to CZT(S, Se), suitable direct bandgaps, and high absorption coefficients; also, quaternary Cu_2-II-SnS_4 (II = Co^{2+}, Fe^{2+}, Ni^{2+}, Mn^{2+}) compounds are considered to be important potential solar cell materials [11]. The best PCEs for kesterite CZTS and CZTSe-based solar cells have been reported to be 8.4% and 12.6%, respectively [12, 13]. The quaternary material CZT(S, Se) can thus lead a new generation of economic and environmentally benign photovoltaic (PV) devices with sufficient availability of their constituent elements. One of the major factors in the success of the synthesis of this kind of solar cell is precise control of secondary phases and deep defect levels as well as the mastery of high-quality phase formation.

Another key factor in optimizing the PCE of CZTS-based solar cells to be mature as its counterpart CIGS-based solar cells is the bandgap grading. It has been shown that the addition of iron in the CZTS lattice can tune its bandgap and hence can improve its PCE [14, 15]. The ionic radius of Zn^{2+} (0.64 Å) and Fe^{2+} (0.66 Å) [16] is almost similar, and iron shows good miscibility in the CZTS lattice. The Fe/Zn alloying is therefore possible and can lead to solid-state materials of the type $Cu_2Zn_{1-x}Fe_xSnS_4$ ($0 < x < 1$). These materials are composed of comparatively cheap, abundant, and environmentally friendly elements. The bandgap can be tuned

across the visible range of solar radiation, which makes them potentially useful in a variety of electronic, optoelectronic, and magnetoelectronic applications [17]. One of the best ways to study the role of bandgap grading or iron addition in optimizing the PCE of these solar cells is to use numerical simulations. Numerical simulation is an important step that can allow understanding different ways to improve the PCE of solar cells as well as a better comprehension of the physics involved in their design and their operation. Numerical simulations of CZTS-based solar cells have been reported already [18–21]. Khattak et al. reported the numerical baseline for high-efficiency CFTS-based solar cells using the SCAPS software and found an optimized simulated solar cell with 19.97% of PCE [22]. Konan et al. found a PCE of 22.33% of an optimized simulated CFTS-based solar cell by SCAPS [23]. But there is a lack of reports on the numerical simulations of CZFTS-based solar cells.

In this study, numerical results were recorded using the Analysis of Microelectronic and Photonic Structures (wxAMPS-1D) program to evaluate and improve CZFTS solar cells' performances. The ZnO:Al/ZnO/CdS/CZFTS/Mo solar cells with different mole fractions of iron were simulated and analyzed. The analysis deals with the effect of the iron content on the overall electrical performance of solar cells. The variations of several structural and physical parameters of the buffer layer CdS and absorber layer CFTS on the overall electrical characteristics of the solar cells were also investigated. The results obtained can serve as a basis for the design and manufacture of high-efficiency CZFTS solar cells. Details of the structure and simulation procedure of the cell are stated in the following sections.

2. Simulation Program and Device Structure

2.1. Simulation Program. In this study, numerical modeling of CZFTS thin-film solar cells was carried out by one-dimensional device simulation program wxAMPS. The structural and physical parameters of each layer of the cell were introduced into the program as input parameters to the simulation. Developed by Fonash and his group at the Pennsylvania State University, it was created first as AMPS to examine a variety of device structures such as homojunction and heterojunction p-n and p-i-n, solar cells, detectors, and microelectronic structures, multijunction structures, compositionally graded detectors, Schottky barrier devices with optional back layer, and novel microelectronic, photovoltaic, and optoelectronic structures [24, 25]. It was originally developed for crystalline Si, GaAs, and multiple models. Later, standard models for polycrystalline devices at the level of best efficiencies were developed such as CdTe, CIGS, and a-Si [26]. The AMPS simulation program can simulate up to 30 layers, in addition to two layers corresponding to the front and the back contacts [24]. It incorporates all recombinations and charges defect mechanisms compared to other simulation programs. Outputs, such as current-voltage characteristics under dark and illumination conditions, quantum efficiency, generation and recombination profiles, electric field distribution, free and trapped carrier densities, energy band diagram at equilibrium, and under illumination, can be recorded from a simulation by AMPS. All this information is computed by AMPS based on Poisson's equation and the continuity equation for free electrons and free holes [24]. Several extensions have been implemented in a new shape named wxAMPS by the Angus Rockett group at the University of Illinois. Beyond the original AMPS kernel, wxAMPS incorporates two tunneling models and can simulate an unlimited number of layers and graded solar cells. Five separate input windows are combined into one for quick editing and viewing. The iteration times were reduced, and the convergence has been significantly improved [26–28].

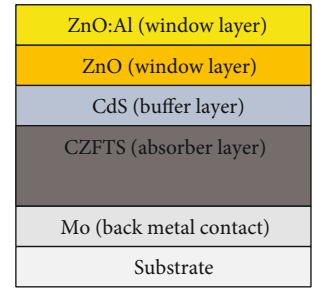

Figure 1: CZFTS solar cell structure used in this work.

2.2. Device Structure and Input Parameters. The CZFTS structure used for our simulations consists essentially of the following layers: a ZnO:Al window layer, ZnO window layer, CdS buffer layer, CZFTS absorber layer, and Mo back layer acting as metal contact. Figure 1 illustrates the vertical cross-section of the cell used in this work. The device is illuminated from the front ZnO:Al to the end of the device with the default AM1.5G illumination spectrum for all simulations. The default working temperature was fixed at 300 K. The basic physical and optoelectronic input parameters used in simulations are listed in Table 1. These parameters were chosen from experimental measurements from AZoM and literature [17, 29–34]. The front surface reflectivity and the back surface reflectivity are set to 0.1 and 0.8, respectively, to reflect experimental quantum efficiency data.

3. Results and Discussion

3.1. Calculation of the CZFTS Bandgap Energy. The addition of iron in CZTS lattice tunes its bandgap. As the iron content increases in the compound, its bandgap decreases according to the bandgap bowing model described by the following equation and depicted in Figure 2 [34].

$$E_g^{\mathrm{CZFTS}}(y) = yE_g^{\mathrm{CFTS}} + (1-y)E_g^{\mathrm{CZTS}} - by(1-y), \quad (1)$$

where y is the iron content and b is the specific optical bowing constant which describes the degree of nonlinearity and is the result of combined effects; $b = b_1 + b_2 + b_3$ where b_1 is related to electron exchange charge and redistribution, b_2 is the effect of crystal lattice variation on band structure, and b_3 is the internal structural relaxation of the anion-cation bond lengths and angles [15, 34, 35]. The bandgap of CZTS

Table 1: Input parameters used in our simulations.

Parameters Material	Window layer ZnO:Al	Window layer ZnO	Buffer layer CdS	Absorber layer $CZ_{1-y}F_yTS$
Thickness (μm)	0.3	0.1	0.05	2
Bandgap energy (eV)	3.5	3.4	2.42	Varying
Electron affinity (eV)	4.5	4.5	4.2	4.5
Dielectric permittivity (relative)	8.5	8.5	8.9	10
CB effective density of states (cm^{-3})	2.2×10^{18}	2.2×10^{18}	2.2×10^{18}	2.2×10^{18}
VB effective density of states (cm^{-3})	1.8×10^{19}	1.8×10^{19}	1.8×10^{19}	1.8×10^{19}
Electron mobility (cm^2/Vs)	50	200	350	50
Hole mobility (cm^2/Vs)	25	180	40	50
Donor density N_D (cm^{-3})	1×10^{20}	1×10^{18}	1×10^{17}	0
Acceptor density N_A (cm^{-3})	0	0	0	1×10^{16}
Gaussian defect N_G (cm^{-3})	1×10^{18}	1×10^{17}	1×10^{18}	1×10^{13}
Absorption coefficient (cm^{-1})	From SCAPS	From SCAPS	From SCAPS	Varying

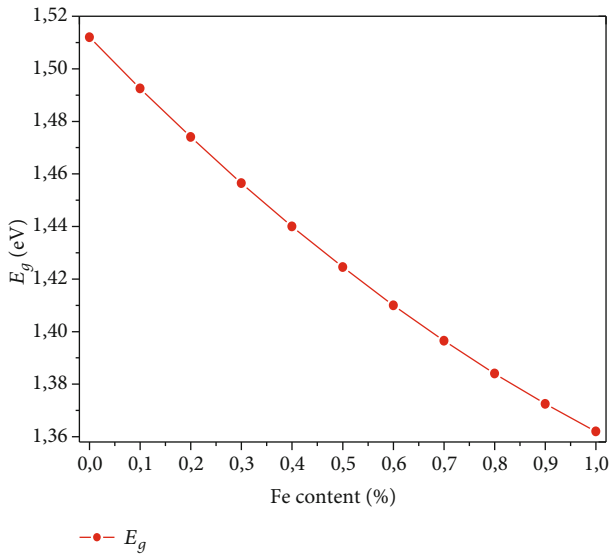

Figure 2: The plot of the variation of the bandgap with increasing Fe content.

and the corresponding iron phase CFTS were set at 1.512 eV and 1.362 eV, respectively. The bowing constant b was chosen as 0.05. A small value of b indicates good miscibility of the alloying constituents [34, 36].

The parabolic trend observed in the bandgap as Fe content increases in Figure 2 could be attributed to both electronegativities of Zn and Fe atoms and the transition from kesterite to stannite phase [34].

3.2. Effect of Iron Content on Output Parameters. The effect of iron content was evaluated by varying its value from 0 to 1 by step of 0.1. Figure 3(a) shows the variations in electrical parameters and quantum efficiency due to the change in iron fraction mole values of different solar cells. It is seen that the values of the short circuit current density (Jsc), the fill factor (FF), and the power conversion efficiency (η) increase with the Fe content in the compound until the maximum value of 1, while the open-circuit voltage (Voc) decreases linearly with it. The increase in Fe content narrowed the bandgap energy of the material and improves its absorption profile. The absorption of more photons can allow generating a significant amount of electron-hole pairs and therefore an important collection of free electrons at the front contact of the cell. This significantly improves the values of Jsc and PCE. Contrariwise, a decrease in bandgap energy can reduce the Schottky barrier height between the absorber layer and the back contact layer and can allow strong recombination of the charge carriers. This phenomenon can affect the value of Voc. There is an increase in the QE with the increase of Fe content due to the improvement in the absorption coefficients. Figure 3(b) shows in real value the variations of J-V characteristics of solar cells with different fraction mole values of iron. It is well seen that the value of Jsc increases while that of Voc decreases.

As the PCE increases substantially with the Fe content up to the value of 1, this layer (CFTS) has been chosen for the solar cell optimization.

3.3. Effect of Physical Parameters

3.3.1. In CdS Buffer Layer. To study the effect of carrier concentration in the CdS buffer layer on the electrical outputs of the solar cell, its value has been varied from 1×10^{16} to 1×10^{17} cm^{-3} which corresponds to experimental values of Cu-doped CdS material [37]. The variations of solar cell electrical parameters for different carrier concentrations can be seen in Figure 4(a). It is seen that the PCE and FF increase when the carrier concentration increases while the Voc and the Jsc slightly decrease. The decrease in the Voc values is probably due to the nonradiative recombination process which starts at the CdS/CFTS interface. This phenomenon increases the saturation current density resulting in a decrease in the value of Voc [38]. When the carrier concentration increases in the CdS buffer layer, the diffusion length of charge carriers decreases, and this contributes to narrow the value of Jsc

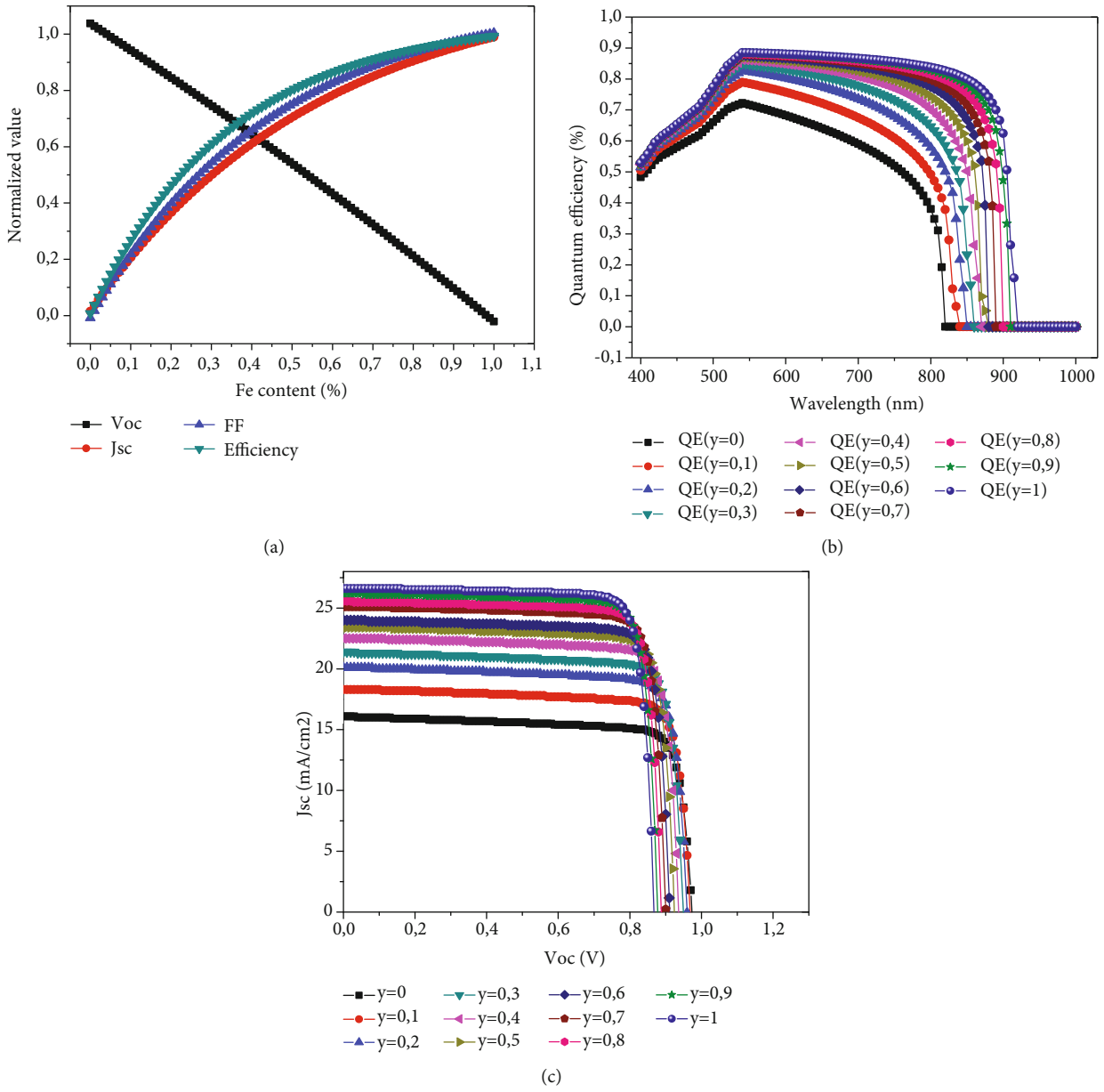

FIGURE 3: (a) Calculated normalized output parameters and quantum efficiency of the CZFTS solar cells as a function of the Fe content and (b) variation of J-V characteristics with Fe content.

[39]. The increase observed in the PCE values is due to the lowering of the barrier potential at the CdS/CFTS heterojunction interface when the carrier concentration increases, thus leading to an enlargement of the space charge region [40]. This situation allows a good collection of photogenerated carriers and can increase the PCE [41]. The best value of carrier concentration in the CdS buffer layer giving the best PCE is chosen as $1 \times 10^{17}\,\text{cm}^{-3}$.

The CdS buffer layer thickness was varied from 0.02 to $0.12\,\mu$m to find its suitable value in the improvement of PCE. The carrier concentration was fixed at the result of the previous simulation, that is, $1 \times 10^{17}\,\text{cm}^{-3}$. Figure 4(b) shows the different variations in the solar cell electrical parameters as a function of the thickness. It is observed that all output parameters exhibit the same behavior. They are almost unchanged between 0.02 and $0.047\,\mu$m, increasing substantially to $0.05\,\mu$m before stabilizing above. The improvement in output parameters with increasing buffer layer thickness is due to the increasing amount of photon absorption outside the hole diffusion length, reducing therefore the recombination rate [42]. At the same time, the values of Voc and Jsc are both affected by the concentration of carriers in the buffer layer which does not allow them to increase further, and thus, they start to stabilize after a certain thickness [40].

3.3.2. In CFTS Absorber Layer. The influence of the CFTS absorber layer thickness was studied by varying its value from

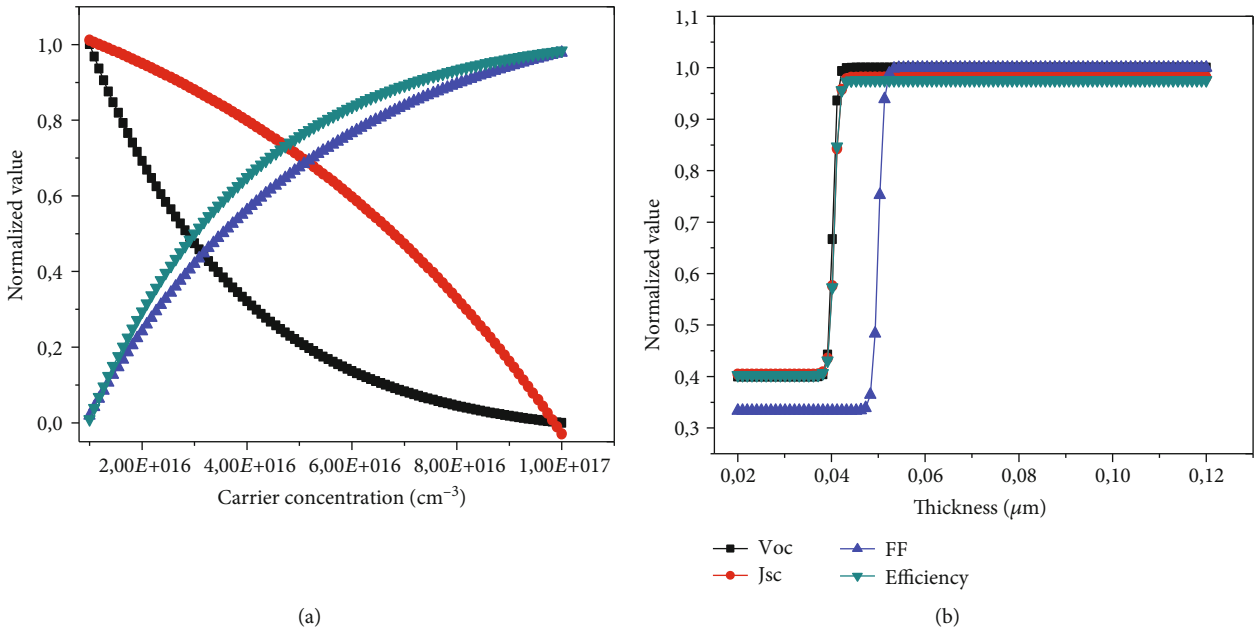

FIGURE 4: Calculated normalized output parameters of CFTS solar cell as a function (a) of carrier concentration and (b) of the thickness in the CdS buffer layer.

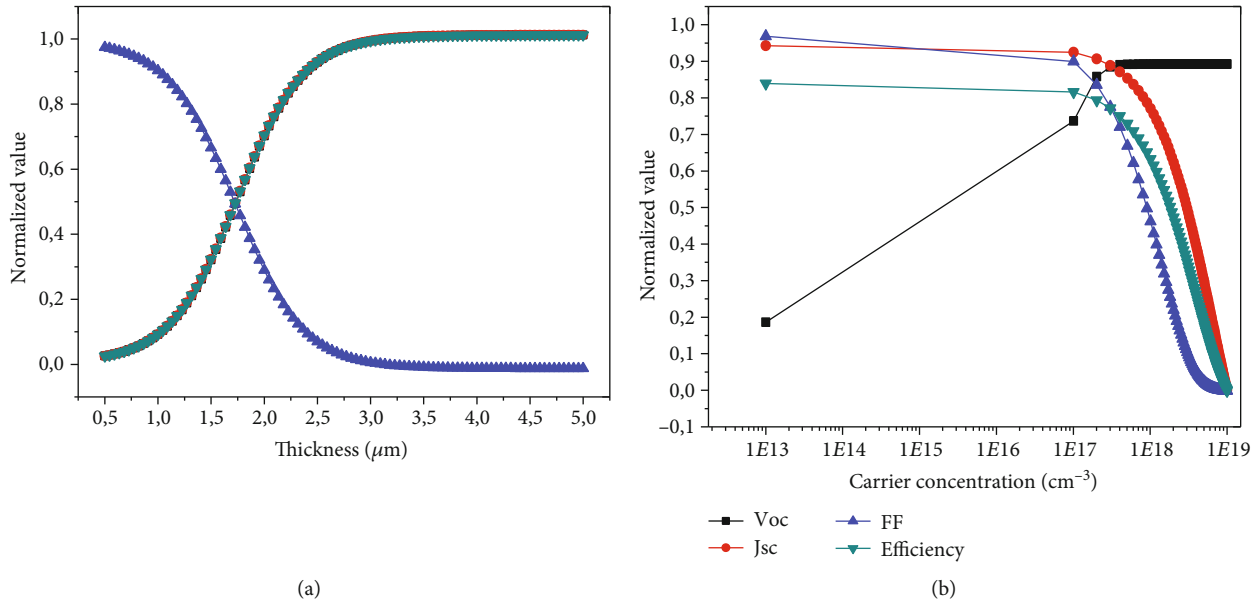

FIGURE 5: Calculated normalized output parameters of CFTS solar cell as a function (a) of the thickness and (b) of carrier concentration in the CFTS absorber layer.

0.5 to 5 μm by step of 0.5 μm. The carrier concentration and thickness of the CdS buffer layer were kept constant at 1×10^{17} cm^{-3} and 0.05 μm, respectively, as they were found as optimal values by previous simulations. All other parameters were kept unchanged. Figure 5(a) exhibits the effect of CFTS absorber layer thickness on the electrical characteristics of the whole cell. As absorber thickness increases, short current density (Jsc), open-circuit voltage (Voc), and power conversion efficiency (PCE) increase up to an optimal value of 2.6 μm and start stabilizing beyond. The fill factor (FF) decreases following an opposite trend. The increase in Jsc, Voc, and PCE is mainly due to the absorption of a greater number of longer wavelength photons, which in some way can affect the amount of photogenerated carriers [22]. A significant amount of electron-hole pairs is generated by an enhanced absorption of photons, and so, a good number of free carriers can be collected at the front; this improves the Jsc values and therefore the PCE. Consequently, a significant number of photogenerated carriers can affect their mobility and this will foster their recombination before reaching the front contact and be collected. This situation can explain the decrease in FF values.

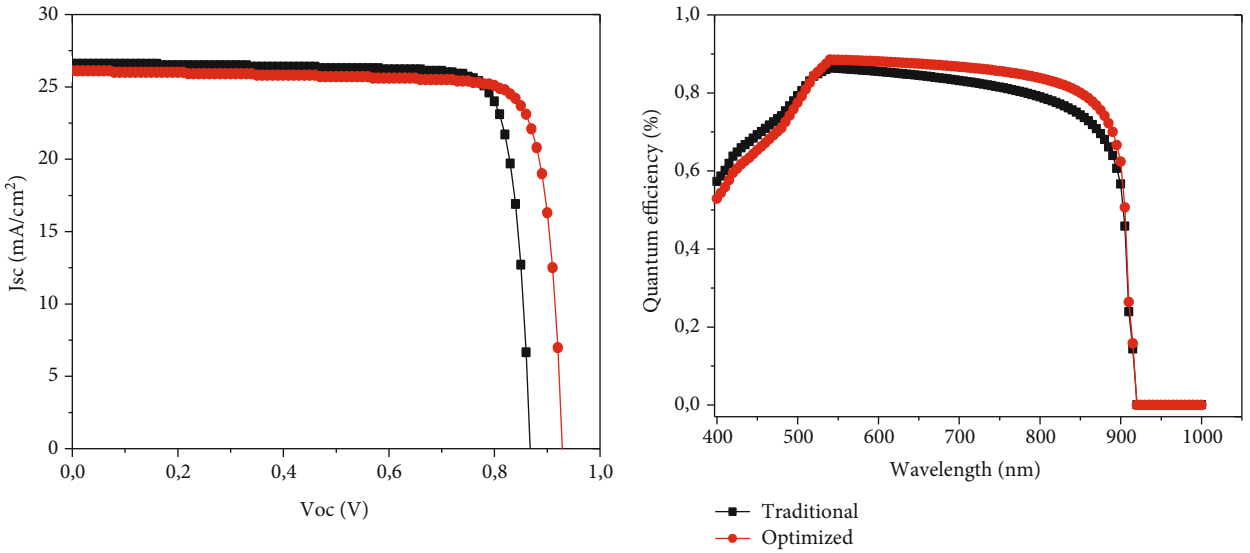

Figure 6: J-V characteristics and quantum efficiency of traditional and optimized CFTS solar cells.

Carrier concentration in the CFTS absorber layer was varied from 1×10^{13} to 1×10^{19} cm^{-3} as shown in Figure 5(b) to see its variations on electrical outputs of the cell.

It can be seen in Figure 5(b) that Jsc, FF, and PCE are nearly unchanged when carrier concentration varies between 1×10^{13} and 1×10^{17} cm^{-3} and start decreasing above. On the other side, the Voc increases from 1×10^{13} to 1.5×10^{17} cm^{-3} and stabilizes beyond. The decrease in Jsc can be explained by the creation of new recombination centers into the layer as the carrier concentration increases. This situation enhances the recombination process which reduces the ratio of photocarriers to be collected at the front contact. This can also cause a drop in the FF values and therefore the PCE. A higher number of carrier concentrations in the CFTS absorber layer cause a drop of the saturation current of the cell which decreases when the carrier density increases; this decrease leads to an improvement in Voc values according to the simple p-n junction model. Finally, the value 1×10^{17} cm^{-3} was found to be the optimal value of the carrier concentration in the absorber layer.

3.4. Comparison between the Traditional and the Optimized CFTS-Based Solar Cell. A thickness of 0.05 μm and a carrier concentration of 1×10^{17} cm^{-3} in the buffer layer, as well as a thickness of 2.6 μm and a carrier density of 1×10^{17} cm^{-3} in the absorber layer, were found to be the best parameter values of our previous simulations. A simulation using these optimal parameter values has been done to evaluate their contribution to the traditional case. J-V characteristics and quantum efficiencies of the traditional and optimized CFTS solar cells are shown in Figures 6(a) and 6(b), respectively. The optimized values of solar cell parameters for CdS buffer and CFTS absorber layers for this simulation and that of the traditional case are summarized in Table 2. The values are comparable with those of other authors [22, 23]. A significant improvement in Voc even if the Jsc decreases slightly is seen in Figure 6(a). A slight increase in photon absorption in the visible range for the optimized structure compared to the traditional case is also seen in Figure 6(b).

Table 2: Output parameters for traditional and optimized CFTS solar cell.

Structure	Voc (V)	Jsc (mA/cm^2)	FF (%)	PCE (%)
Traditional	0.8676	26.6364	84.6216	19.55
Optimized	0.9289	26.0976	83.9344	20.35

4. Conclusion

In this work, the baselines of ZnO:Al/ZnO/CdS/CZFTS/Mo solar cells have been analyzed via the wxAMPS software. The effect of iron was first evaluated, and CZFTS-based solar cells with a fraction mole value of iron equal to 1 showed the best performance. Then, variations of different parameters of the CdS buffer and CFTS absorber layers on electrical output parameters have been studied. Promising optimized results were achieved with a PCE of 20.35%, a short circuit density (Jsc) of 26.09 mA/cm^2, an open-circuit voltage (Voc) of 0.93 V, and a fill factor (FF) of 83.93%. These promising results can bring researchers to have a broad interest in the manufacture of high efficient CZFTS-based solar cells. But to better understand this kind of solar cell, it is important and even necessary to conduct several other simulations taking into account other physical or chemical parameters, different other conditions, and different other structure configurations to find the one exhibiting the best performance.

Data Availability

The CZ0F1TS.dev and CZFTS.dev data used to support the findings of this study are available from the corresponding author upon request.

Conflicts of Interest

The authors declare that there is no conflict of interest regarding the publication of this paper.

Acknowledgments

The authors acknowledge Prof. Angus Rockett, Dr. Yimming Liu of UIUC, and Prof. Stephen Fonash of the PSU for providing the wxAMPS simulation software.

References

[1] K. Ramasamy, M. A. Malik, and P. O'Brien, "Routes to copper zinc tin sulfide Cu_2ZnSnS_4 a potential material for solar cells," *Chemical Communications*, vol. 48, no. 46, pp. 5703–5714, 2012.

[2] S. Bag, O. Gunawan, T. Gokmen, Y. Zhu, T. K. Todorov, and D. B. Mitzi, "Low band gap liquid-processed CZTSe solar cell with 10.1% efficiency," *Energy & Environmental Science*, vol. 5, no. 5, pp. 7060–7065, 2012.

[3] A. Walsh, S. Chen, S. H. Wei, and X. G. Gong, "Kesterite thin-film solar cells: advances in materials modelling of Cu_2ZnSnS_4," *Advanced Energy Materials*, vol. 2, no. 4, pp. 400–409, 2012.

[4] J. Li, D. B. Mitzi, and V. B. Shenoy, "Structure and electronic properties of grain boundaries in earth-abundant photovoltaic absorber $Cu_2ZnSnSe_4$," *ACS Nano*, vol. 5, no. 11, pp. 8613–8619, 2011.

[5] J. Wang, X. Xin, and Z. Lin, "Cu_2ZnSnS_4 nanocrystals and graphene quantum dots for photovoltaics," *Nanoscale*, vol. 3, no. 8, pp. 3040–3048, 2011.

[6] D. A. R. Barkhouse, O. Gunawan, T. Gokmen, T. K. Todorov, and D. B. Mitzi, "Device characteristics of a 10.1% hydrazine-processed $Cu_2ZnSn(Se,S)_4$ solar cell," *Progress in Photovoltaics: Research and Applications*, vol. 20, no. 1, pp. 6–11, 2012.

[7] T. Washio, T. Shinji, S. Tajima et al., "6% efficiency Cu_2ZnSnS_4-based thin film solar cells using oxide precursors by open atmosphere type CVD," *Journal of Materials Chemistry*, vol. 22, no. 9, pp. 4021–4024, 2012.

[8] S. Ahmed, K. B. Reuter, O. Gunawan, L. Guo, L. T. Romankiw, and H. Deligianni, "A high efficiency electrodeposited Cu_2ZnSnS_4 solar cell," *Advanced Energy Materials*, vol. 2, no. 2, pp. 253–259, 2012.

[9] Q. Guo, H. W. Hillhouse, and R. Agrawal, "Synthesis of Cu_2ZnSnS_4 nanocrystal ink and its use for solar cells," *Journal of the American Chemical Society*, vol. 131, no. 33, pp. 11672-11673, 2009.

[10] K. Wang, O. Gunawan, T. Todorov et al., "Thermally evaporated Cu_2ZnSnS_4 solar cells," *Applied Physics Letters*, vol. 97, no. 14, pp. 143508–143508-3, 2010.

[11] Y. Cui, R. Deng, G. Wang, and D. Pan, "A general strategy for synthesis of quaternary semiconductor Cu_2MSnS_4 (M = Co^{2+}, Fe^{2+}, Ni^{2+}, Mn^{2+}) nanocrystals," *Journal of Materials Chemistry*, vol. 22, no. 43, article 23136, 2012.

[12] B. Shin, O. Gunawan, Y. Zhu, N. A. Bojarczuk, S. J. Chey, and S. Guha, "Thin film solar cell with 8.4% power conversion efficiency using an earth-abundant Cu_2ZnSnS_4 absorber," *Progress in Photovoltaics: Research and Applications*, vol. 21, no. 1, pp. 72–76, 2013.

[13] W. Wang, M. T. Winkler, O. Gunawan et al., "Device characteristics of CZTSSe thin-film solar cells with 12.6% efficiency," *Advanced Energy Materials*, vol. 4, no. 7, article 1301465, 2014.

[14] R. Haight, A. Barkhouse, O. Gunawan et al., "Band alignment at the $Cu_2ZnSn(S_xSe_{1-x})_4$/CdS interface," *Applied Physics Letters*, vol. 98, no. 25, pp. 253502–253507, 2011.

[15] S. Chen, A. Walsh, J. H. Yang et al., "Compositional dependence of structural and electronic properties of $Cu_2ZnSn(S,Se)_4$ alloys for thin film solar cells," *Physical Review B: Condensed Matter and Materials Physics*, vol. 83, no. 12, p. 125201, 2011.

[16] R. D. Shannon, "Bond distances in sulfides and a preliminary table of sulfide crystal radii," *Industrial Chemistry Library*, vol. 2, pp. 53–70, 1981.

[17] P. Kevin, M. A. Malik, S. Mcadams, and P. O'Brien, "Synthesis of nanoparticulate alloys of the composition $Cu_2Zn_{1-x}Fe_xSnS_4$: structural, optical, and magnetic properties," *Journal of the American Chemical Society*, vol. 137, no. 48, pp. 15086–15089, 2015.

[18] M. Patel and A. Ray, "Enhancement of output performance of Cu_2ZnSnS_4 thin film solar cells-a numerical simulation approach and comparison to experiments," *Physica B*, vol. 407, no. 21, pp. 4391–4397, 2012.

[19] W. Zhao, W. Zhou, and X. Miao, "Numerical simulation of CZTS thin film solar cell," in *2012 7th IEEE International Conference on Nano/Micro Engineered and Molecular Systems (NEMS)*, vol. 7, pp. 502–505, Kyoto, Japan, March 2012.

[20] S. Çetinkaya, "Study of electrical effect of transition-metal dichalcogenide-MoS_2 layer on the performance characteristic of Cu_2ZnSnS_4 based solar cells using wxAMPS," *Optik*, vol. 181, pp. 627–638, 2019.

[21] J. H. Nkuissi Tchognia, Y. Arba, K. Dakhsi et al., "Optimization of the output parameters in kesterite-based solar cells by AMPS-1D," in *2015 3rd International Renewable and Sustainable Energy Conference (IRSEC)*, pp. 1–6, Marrakech, Morocco, December 2015.

[22] Y. H. Khattak, F. Baig, S. Ullah, B. Marí, S. Beg, and H. Ullah, "Numerical modeling baseline for high efficiency (Cu_2FeSnS_4) CFTS based thin film kesterite solar cell," *Optik*, vol. 164, pp. 547–555, 2018.

[23] F. K. Konan, H. J. Tchognia Nkuissi, and B. Hartiti, "Numerical simulations of highly efficient Cu_2FeSnS_4 (CFTS) based solar cells," *International Journal Of Renewable Energy Research*, vol. 9, pp. 1865–1872, 2019.

[24] J. Arch, J. Hou, W. Howland et al., *A Manual for AMPS-1D BETA Version 1.00*, The Pennsylvania State University, 1997.

[25] S. J. Fonash, *Solar Cell Device Physics*, Elsevier, 2nd edition, 2010.

[26] Y. Liu, Y. Sun, and A. Rockett, "A new simulation software of solar cells—wxAMPS," *Solar Energy Materials and Solar Cells*, vol. 98, pp. 124–128, 2012.

[27] W. Chen, X. Huang, Q. Cheng, C. Chen, D. Yun, and F. Zhang, "Simulation analysis of heterojunction ZnO/CdS/Cu(In,-Ga)Se_2 thin-film solar cells using wxAMPS," *Optik*, vol. 127, no. 1, pp. 182–187, 2016.

[28] J. Liu, M. Zhang, and X. Feng, "Simulation of graded bandgap on the performance of back-wall superstrate CIGS solar cells," *Optik*, vol. 172, pp. 1172–1178, 2018.

[29] "Copper Zinc Tin Sulfide (Cu2ZnSnS4) Semiconductors," 2013, February 2020, https://www.azom.com/article.aspx?ArticleID=8503.

[30] "Zinc Oxide (ZnO) Semiconductors," 2013, February 2020, https://www.azom.com/article.aspx?ArticleID=8417.

[31] "Cadmium Sulfide (CdS) Semiconductors," 2013, February 2020, https://www.azom.com/article.aspx?ArticleID=8407.

[32] S. Adachi, "Physical properties: Compiled Experimental Data," in *Copper Zinc Tin Sulfide-Based Thin-Film Solar Cells*, pp. 149–179, Wiley Online Library, 2015.

[33] S. Adachi, "Earth-Abundant Materials for Solar Cells: Cu2-II-IV-VI4 Semiconductors," *Earth-Abundant Mater. Sol. Cells Cu_2-II-IV-VI_4 Semicond*, pp. 1–462, Wiley, 2015.

[34] D. B. Khadka and J. H. Kim, "Structural transition and band gap tuning of $Cu_2(Zn,Fe)SnS_4$ chalcogenide for photovoltaic application," *Physical Chemistry C*, vol. 118, no. 26, pp. 14227–14237, 2014.

[35] J. E. Bernard and A. Zunger, "Electronic structure of ZnS, ZnSe, ZnTe, and their pseudobinary alloys," *Physics Review*, vol. 36, no. 6, pp. 3199–3228, 1987.

[36] Z. Shadrokh, A. Yazdani, and H. Eshghi, "Solvothermal synthesis of Cu_2Zn_1−xFexSnS_4 nanoparticles and the influence of annealing conditions on drop-casted thin films," *Semiconductor Science and Technology*, vol. 31, no. 4, article 045004, 2016.

[37] H. W. Brandhorst, *Impurity profile and energy band diagram for the cuprous sulfide-cadmium sulfide heterojunction*, National Aeronautics and Space Administration, Washington, 1969.

[38] A. Kanevce, M. O. Reese, T. M. Barnes, S. A. Jensen, and W. K. Metzger, "The roles of carrier concentration and interface, bulk and grain-boundary recombination for 25% efficient CdTe solar cells," *Journal of Applied Physics*, vol. 121, no. 21, p. 214506, 2017.

[39] S. Kolsi, M. Ben Amar, H. Samet, and A. Ouali, "Effect of Gaussian doping profile on the performance of a thin film polycrystalline solar cell," *EPJ Web of Conferences*, vol. 29, article 00025, 2012.

[40] F. A. Jhuma and M. J. Rashid, "Simulation study to find suitable dopants of CdS buffer layer for CZTS solar cell," *Journal of Theoretical and Applied Physics*, vol. 14, no. 1, pp. 75–84, 2020.

[41] S. Dabbabi, T. B. Nasr, and N. Kamoun-Turki, "Parameters optimization of CIGS solar cell using 2D physical modeling," *Results in Physics*, vol. 7, pp. 4020–4024, 2017.

[42] M. A. Green, *Solar Cells: Operating Principles, Technologies and System Applications*, Prentice Hall, Eaglewood Cliffs, 1982.